Peak Input Torque Minimization of a Flapping Wing Mechanism for MAVs

Conference Paper *in* Collection of Technical Papers - AIAA/ASME/ASCE/AHS/ASC Structures, Structural Dynamics and Materials Conference · April 2013

DOI: 10.2514/6.2013-1787

2 authors:

Hai-Jun Su
The Ohio State University
165 PUBLICATIONS **2,934** CITATIONS
SEE PROFILE

Mark Ryan
Milwaukee School of Engineering
3 PUBLICATIONS **22** CITATIONS
SEE PROFILE

AIAA 2013-1787

Peak Input Torque Minimization of a Flapping Wing Mechanism for MAVs

Mark Ryan[*] **Venkatasubramanian Kalpathy Venkiteswaran**[†] **Hai-Jun Su**[‡]
Department of Mechanical and Aerospace Engineering
The Ohio State University, Columbus, OH 43210

Flapping wing micro air vehicles (MAVs) are desired for surveillance and reconnaissance in confined spaces, and should exhibit small scale flight with the following abilities: obstacle avoidance, hovering, and slow flight speed. One of the major components of MAVs is the flapping mechanism, which actuates wings to generate sufficient lift and propulsion force. The use of compliant elements in flapping wing MAVs is a possible solution to the decreased power transmission inherently present in the scaling of traditional rigid body mechanisms. To demonstrate the effectiveness of compliant elements, an extension spring and compliant joint were incorporated into the University of Maryland's Small Bird MAV. The motor torque was derived in terms of the rigid body mechanics, and compliant parameters optimized using an interior point algorithm to minimize the peak motor torque throughout the flapping cycle. Under the assumption of constant aerodynamic load on the wings, the extension spring and compliant joint mechanisms resulted in a 89.25% and a 97.1% reduction in the motor torque from the rigid body mechanism, respectively. To validate this analytical solution, the mechanisms were modeled in MSC Software's ADAMS simulation engine.

I. Introduction

The Defense Advanced Research Projects Agency (DARPA) has established a MAV and NAV program[10] for the development of small size autonomous flying air vehicles. MAVs are defined as air vehicles which are about 15 cm in length, 100 g in weight (including payload), and have a flight duration between 20 and 60 minutes. NAVs have further reduced requirements of less than 15 cm in length and weigh less than 20 g.[12] The primary focus of the military has been the need for indoor surveillance and reconnaissance within confined or difficult to access areas. Chemical contamination, presence of hazardous material, and threat detection may all play a critical role in a combat environment.[1] Civilian applications may include the need for police and firefighters to inspect unsafe or collapsed buildings for survivors.

In recent years, academia and the Department of Defense (DoD) labs have been devoting more and more resources to MAV research. The design and development of MAVs has focused primary on three different platforms which exhibit active propulsion: fixed wing, rotary wing, and flapping wing. The scaling of current flight vehicles has important implications on aerodynamic performance, miniaturized electromechanical technology, and system integration. The major challenge of scaling down MAVs is decreased efficiency at smaller sizes.[7] This includes the decreased aerodynamic efficiencies at lower Reynolds numbers, and decreased power transmission in traditional mechanisms.

Fixed wing and rotary based air vehicles suffer from the unsteady aerodynamics present in the low Reynolds number range of insect flight. Insects and small birds are able to generate lift and thrust forces, which are 2 to 12 times their body weight.[12] Due to the demonstrated efficiency of lift production and their ability to generate a wide variety of flight maneuvers, insect-like kinematics have been widely pursued. The focus of this paper will be two-winged flapping flight, as it best matches the goals set by DARPA. Even though insect-like kinematics may provide a better long term solution to the scaling of aerodynamics, the

[*]Graduate Research Associate
[†]Graduate Research Associate
[‡]Assistant Professor, su.298@osu.edu, AIAA member

design challenges are numerous. An example of flapping wing flight is AeroVironment's Nano Hummingbird.[5] Recently Ryan and Su[13,14] surveyed and classified various designs of flapping wing mechanisms worldwide using adjacency matrices. Many of the designs use compliant mechanisms.

In this paper, we will demonstrate the use of compliant elements, in a flapping wing mechanism, as a way minimize the peak motor torque. Previous work in this field includes several designs of four-bar linkages, which imitate the flapping cycle of an insect. Madangopal et al.[8] developed a four-bar flapping wing mechanism which utilized an extension spring. Using a quasi-steady aerodynamic model, it was shown that the load variation experienced by the motor could be reduced. Tantanawat[15] analyzed the same mechanism provided by Mandangopal and demonstrated the difference in power consumption between a rigid body and extension spring mechanism. The applied aerodynamic load was simplified to a constant load, which was always perpendicular to the wing. It is concluded that a compliant mechanism is a good choice to reduce the power consumption if the load on the mechanism is biased toward one half of the motion cycle. Compliant joints were analyzed by Khatait et al.[6] in a four-bar linkage, as another way to reduce the required input torque.

II. Kinematics of a Flapping Wing Mechanism

In this section, we derive kinematics equations of the flapping wing mechanism used in University of Maryland's Small Bird MAV.

A. The MAV Designs by University of Maryland

The University of Maryland's Small Bird MAV consists of five primary subsystems: the wings, the drive mechanism, the body, the tail, and the actuators/electronics. The overall length of this MAV is $8in.$, the wing span is $13.5in.$, and the weight is $16.3g$. The focus of the transmission design by the University of Maryland was to produce a mechanism which had minimal weight, low cost, and high power transmission efficiency. The primary design requirements for this flapping wing mechanism were a flapping frequency of more than $7Hz$, a flapping stroke of approximately $65°$, transmitting a motor torque no greater than $6.6E-4Nm$, and support a wing area of $2.6E-2m^2$. Additional considerations included design for injection molding such as gate placement and mold flow analysis.

The University of Maryland has produced several iterations of transmission designs, and has improved upon the Small Bird MAV. The Jumbo Bird MAV exhibits a similar transmission design, but incorporates a prismatic joint to induce symmetrical flapping, which is not present in the Small Bird MAV. This improvement was incorporated into the Small Bird MAV for this analysis. The Small Bird MAV utilizes a compliant frame and the Jumbo Bird MAV uses compliant joints. The use of different compliant segments relates to the size of the MAV. Since the Jumbo Bird scales up the size of the transmission, local compliance is chosen to avoid the large and possibly non-linear deflection of a lumped compliance frame. However, the general principle of operation is the same in both mechanisms. The use of elastic elements in the mechanism allows energy to be stored and released during the flapping cycle.

Further assumptions have been made to simplify the analysis. Since the design of the transmission is biplanar, the out-of-plane forces resulting from the motion were insignificant, and the mechanism was considered to be planar. As seen in the classification, only half of the mechanism will be analyzed since the transmission is symmetrical. Additionally, the mass of the structure is relatively small, and the inertial forces have been neglected. Similar to Tantanawat[15] and Gupta,[3] a simplified aerodynamic load was applied to the wing, which allowed the investigation of reduced motor torque.

Pure flapping wing motion produces positive lift during the down stroke and negative lift during the upstroke under zero forward velocity. This MAV generates lift once the initial thrust is provided through a hand launch. Air passes over the air foil shape, which creates a beneficial pressure gradient . The thrust generated from the flapping wing is critical to feed the aerodynamic lift mechanism.[11] Since symmetrical flapping creates minimal lift, large birds reduce the area of their wings by folding them during the upstroke, to decrease the generation of negative lift.

Based on the University of Maryland's design specifications and initial analysis, the maximum allowable aerodynamic load or lift force for the Small Bird MAV was found to be $0.19N$. In this analysis, the aerodynamic load is assumed to be a constant upward force, which is perpendicular and applied to the midpoint of the wing span. This simplified aerodynamic load is associated with an angle of attack that is always positive

and a minimal generation of negative lift.

B. Kinematics of The Flapping Wing Mechanism

As shown in Fig. 1, the flapping mechanism consists of two slider-cranks, OAB and BCD. The coordinate system has been established at the ground pin joint at $\vec{P}_O$. The crank rotates in the positive counter clockwise direction. The numerical values provided are the same as in[2] and are considered constants in this analysis. First, the kinematic constraint equation for the OAB crank-slider will be derived. Then the position of the slider will be used in the second constraint equation of the BCD crank-slider to solve for the remaining unknowns, such as angle ψ and flapping angle ϕ. The kinematic constraint equation of a linkage is obtained from the distance specified between the input and output moving pivots. Solving this equation determines the relationship between the input and output variables.[9]

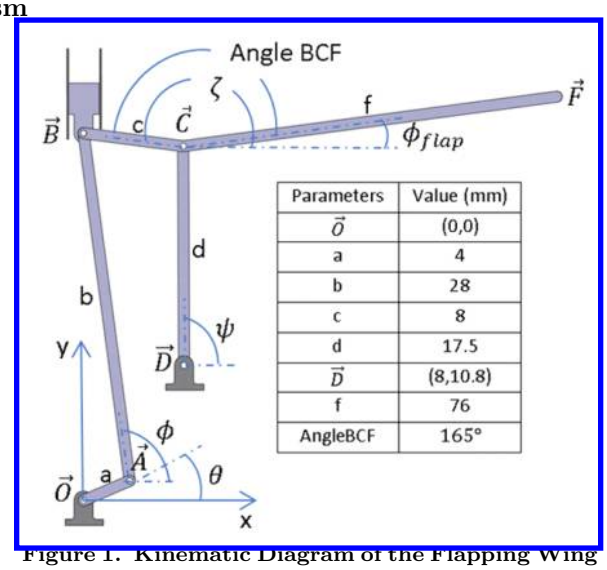

Parameters	Value (mm)
$\vec{O}$	(0,0)
a	4
b	28
c	8
d	17.5
$\vec{D}$	(8,10.8)
f	76
AngleBCF	165°

Figure 1. Kinematic Diagram of the Flapping Wing Mechanism of University of Maryland's Jumbo Bird MAV

The kinematics constraint equation of the slider-crank OAB is

$$\vec{P}_{BA} \cdot \vec{P}_{BA} - b^2 = 0, \tag{1}$$

where $\vec{P}_{BA}$ is the vector connecting the pin joints A and B whose coordinates are given by

$$\vec{P}_A = a \begin{Bmatrix} \cos\theta \\ \sin\theta \end{Bmatrix}, \quad \vec{P}_B = \begin{Bmatrix} e \\ s \end{Bmatrix}.$$

In Eq.(1), θ is the input angle of the motor and s is the output slider parameter. The horizontal offset between $\vec{P}_O$ and $\vec{P}_B$ is the distance e. Substituting values of the crank angle θ into Eq.(1), we can solve for s as

$$s = a\sin\theta + \sqrt{\frac{-a^2}{2} + b^2 - e^2 + 2ae\cos\theta - \frac{1}{2}a^2\cos 2\theta}. \tag{2}$$

The constraint equation of the slider-crank linkage BCD is

$$\vec{P}_{BC} \cdot \vec{P}_{BC} - c^2 = 0 \tag{3}$$

where the coordinates of the pin joint C can be written as

$$\vec{P}_C = \begin{Bmatrix} d_x \\ d_y \end{Bmatrix} + d \begin{Bmatrix} \cos\psi \\ \sin\psi \end{Bmatrix}.$$

Assuming the solution of slider s has been obtained in Eq.(2), we can solve Eq.(3) for the angle ψ as

$$\psi = \arctan(A, B) + \arccos(C/\sqrt{A^2 + B^2}), \tag{4}$$

where A, B, and C are the coefficients of the $\cos\psi$ terms, $\sin\psi$ terms, and the remaining terms of Eq.(3) , respectively. Having solved Eq.(4), the remaining angles are solved as

$$\zeta = \arg(\vec{P}_{BC}), \tag{5}$$

$$\phi_{flap} = \zeta - \angle BCF. \tag{6}$$

The range of angle ψ varies from approximately 90° to 94°. The flapping angle ϕ range is much larger at 60°, where the minimum flapping angle of −13° is reached at a crank angle of 90°, and the maximum flapping angle of 47° is attained at a crank angle of 270°.

Lastly, the position of the midpoint of wing, where the aerodynamic load is to be applied in a normal orientation, is calculated as

$$\vec{P_F} = \vec{P_C} + f \begin{Bmatrix} \cos\phi_{flap} \\ \sin\phi_{flap} \end{Bmatrix}. \tag{7}$$

C. Kinematics of Extension Spring Mechanism

The first modification of the rigid body mechanism is the incorporation of an extension spring. Inspiration for this design is taken from Tantanawat,[15] and applied to the Small Bird MAV mechanism in a similar fashion. As shown in Fig. 2(a), the extension spring is attached to the ground at position $\vec{P_D}$ to $\vec{P_S}$ on the wing spar. Using the kinematics from the rigid body analysis, $\vec{P_S}$ is defined as

$$\vec{P_S} = \vec{P_C} + r \begin{Bmatrix} \cos\phi_{flap} \\ \sin\phi_{flap} \end{Bmatrix}, \tag{8}$$

where r is the distance from $\vec{P_C}$ to $\vec{P_S}$ along the wing spar.

Given the length of the spring is the change in length of the vector from $\vec{P_D}$ to $\vec{P_S}$ and L_0 is the free length of the spring, then the spring displacement can be calculated as

$$\Delta L = |\vec{P}_{SD}| - L_0. \tag{9}$$

This will be used to calculate the force of the spring throughout the flapping cycle. Note that ΔL is dependent on the position of the spring attachment r.

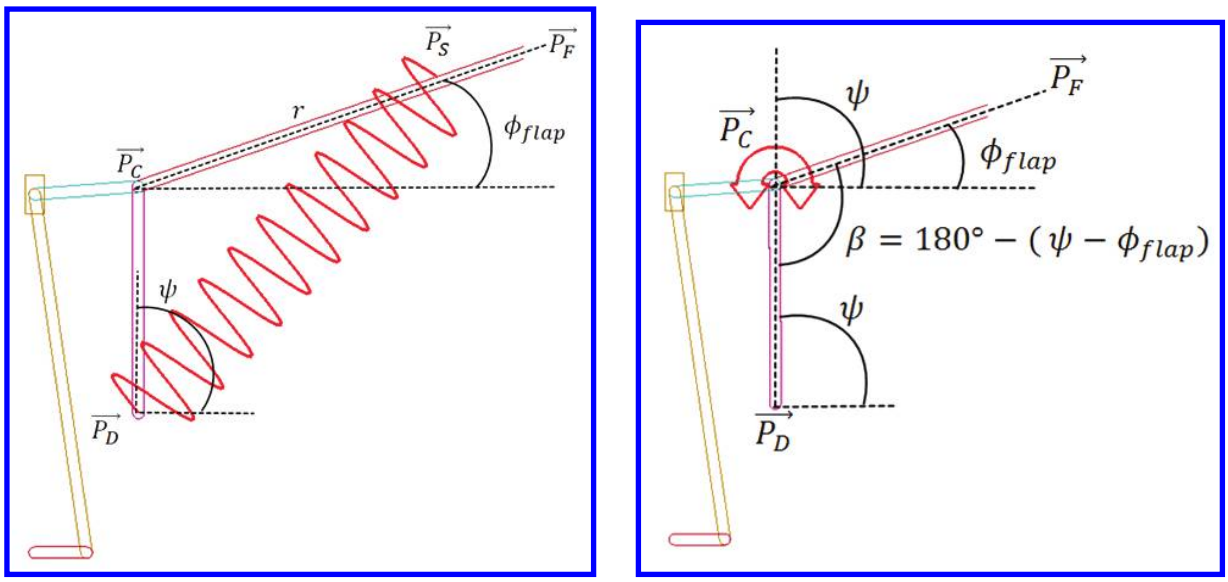

Figure 2. Kinematic Diagram of (a) Extension Spring Mechanism and (b) Compliant Joint Mechanism from ADAMS model

D. Kinematics of Compliant Joint Mechanism

The last design features a compliant joint between the wing spar ($\vec{P_C}$ to $\vec{P_F}$) and the follower ($\vec{P_D}$ to $\vec{P_C}$). This location is chosen since this joint exhibits the largest sweeping motion, and therefore the greatest angular spring displacement. A pseudo-rigid-body-model is used to analyze the compliant joint, which allows flexible segments to be modeled as rigid-body components that have equivalent force-deflection characteristics.[4] The compliant joint being employed is a small-length flexural pivot, and it is modeled as rigid linkages connected by a pin joint with a torsion spring applied. The pivot of the torsion spring is centered at the pin joint and exhibits reaction forces on the associated rigid linkages. A small flexural pivot is implemented between the wing spar and the follower link. An alternative design is to use a short compliant member, which deforms throughout its length to store elastic energy. Using the pseudo-rigid-body-model, the compliant segment would be modeled with two torsional springs at either end of a rigid link. See[13] for more details of these designs. The ADAMS representation of the torsion spring is provided in Fig. 2(b).

The angle between the wing spar and the follower is defined as

$$\beta = 180^\circ - \psi - \phi_{flap} \tag{10}$$

and the angular spring displacement is $\Delta\beta = \beta - \beta_0$ where β_0 is the initial torsion spring angle. These parameters are used to calculate the torsion spring moment, which counteracts the applied aerodynamic load.

III. Minimizing Peak Motor Torque

The required input torque from the motor is derived using the principle of virtual work, which states that if a system of rigid connected rigid bodies is in equilibrium, the total virtual work of the forces acting on the system of rigid connected bodies is zero for any virtual displacement of this system.[9] Virtual displacement is a small imaginary movement of the system over which the applied forces and torques are considered to be constant. All the reactions and internal forces are eliminated and only the work of the applied loads and friction forces need to be considered. In this analysis, it is assumed that the weight of each link and the friction in each joint is negligible compared to the applied forces and torques.

The principle of virtual work also allows the calculation of mechanical advantage for a given mechanism. Mechanical advantage is defined as the ratio of the output torque/force to the input torque/force required.[4] Given the system is in static equilibrium and the power is conserved between the input and the output, then the ratio of forces or velocities is easily determined. Differentiation of the kinematic constraint equation for a given linkage yields the velocities needed to compute mechanical advantage.[9] Power may be calculated by the product of a moment and angular velocity or the dot product of a force and a linear velocity.

In the three cases to be analyzed (rigid body, extension spring, and compliant joint mechanism), the virtual displacement to be used is the angular displacement of the crank ($\delta\theta$). It is assumed that the crank rotates at a constant angular velocity of $1 rad/s$ from the motor. The work done by the motor (applied input torque) must equal the work done by the applied aerodynamic load. This relationship allows the required input torque to be calculated for each of the three cases. These mechanisms were modeled in ADAMS, to check the result of the derived motor torque.

A. Calculate Motor Torque for the Flapping Mechanism

In this section, we calculate the torque from the motor required to actuate the flapping mechanism over a single flap cycle, that is, varying θ between 0 and 2π. The torque equation will be derived for three separate cases using the principle of virtual work.

1. The Rigid Body Mechanism

As previously discussed in Section D, the given flapping wing mechanism is a coupling of crank-slider linkages. To gain insight into the operation of this six-bar linkage, the crank-slider linkage OAB is examined first. Using the conservation of power, the mechanical advantage of the crank-slider is determined and discussed. Then the mechanical advantage of the complete six-bar linkage is derived using the same procedure. The principle of virtual work is applied, and the motor torque for the rigid body mechanism derived.

Starting with the crank-slider linkage, the motor torque is supplied to the crank to counteract F_{slider}, which represents the load applied to the slider by the aerodynamic load. The power equilibrium equation is

$$\tau_{m1}\dot{\theta} = F_{in}a\dot{\theta} = F_{slider}\dot{s}. \tag{11}$$

This readily allows the calculation of the mechanical advantage of the crank-slider linkage OAB. Taking the derivative of the kinematic constraint equation Eq.(1) yields:

$$\dot{s}(s - a\sin\theta) - \dot{\theta}a(s\cos\theta - e\sin\theta) = 0. \tag{12}$$

The mechanical advantage MA of the crank-slider is determined from Eq.(12) by substituting in the solution for s, from Eq.(2), and solving for the ratio of output force and input force from the conservation of power:

$$MA = \frac{F_{out}}{F_{in}} = \frac{\dot{\theta}}{\dot{s}} = \frac{s - a\sin\theta}{a(s\cos\theta - e\sin\theta)}. \tag{13}$$

A seen in Fig. 3, the flapping wing mechanism is driven by the motor torque at the crank to oppose the normal aerodynamic load $0.19N$ at $\vec{P}_F$. The differences in downstroke and upstroke of the flapping stroke

are also highlighted. In this analysis, it is assumed the flapping cycle starts at a crank angle of 0°, and the crank rotates counter-clockwise. The down stroke is from 0° to 90°, and then from 270° to 0° again. The upstroke is from 90° to 270°. The direction of the wing velocity should be noted for each of theses half strokes.

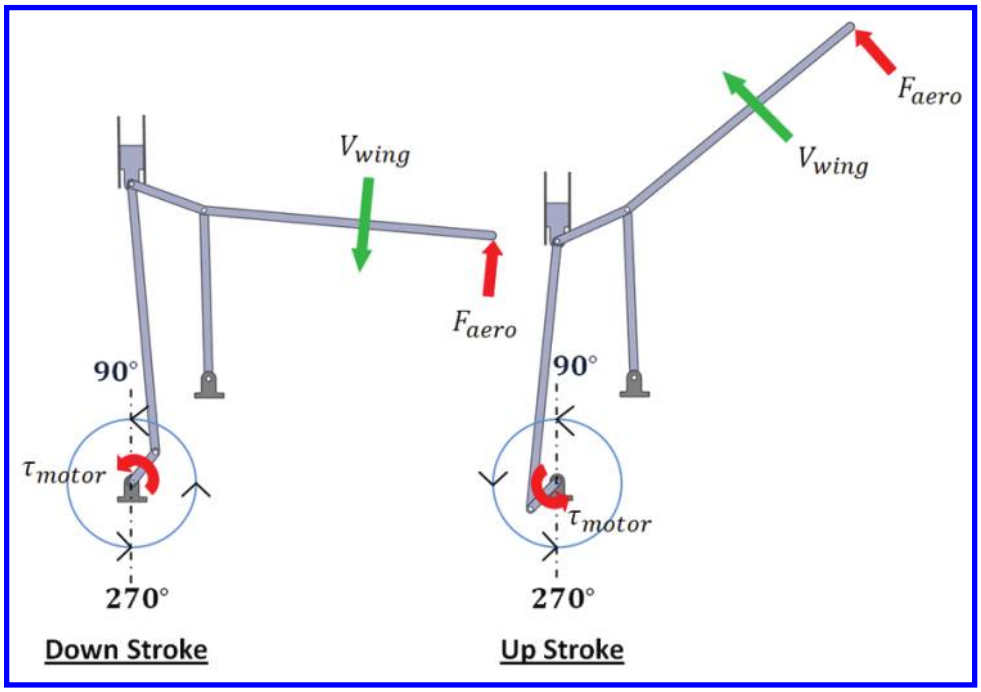

Figure 3. Free Body Diagram and Flapping Cycle

First, the virtual work and the motor torque are derived. Then the mechanical advantage for the complete six-bar linkage is derived in the same manner as the crank-slider. This gives insight into how the geometry could be modified to improve the performance of the mechanism. Using the angular displacement of the crank as the virtual displacement ($\delta\theta$), the virtual work of the complete mechanism is

$$\delta W = \tau_{m1}\dot{\theta}\delta t + \vec{F}_{aero} \cdot \vec{V}_F \delta t = 0, \tag{14}$$

where $\vec{V}_F$ is the linear velocity of $\vec{P}_F$ and the derivative of Eg.(7) with respect to θ. The required motor torque for the rigid body mechanism can be solved from Eg.(14) as

$$\tau_{m1}(\theta) = \frac{-\vec{F}_{aero} \cdot \vec{V}_F}{\dot{\theta}}, \quad \theta \in [0, 2\pi]. \tag{15}$$

The torque resembles a cosine function. The rigid body mechanism exhibited a peak torque of $7.3Nmm$ at a crank angle of 0°, 180°, and 360°. The position of the peak torque at these crank angles is directly related to the mechanism's mechanical advantage throughout the flapping cycle. Referring to Fig. 3, the direction of the wing velocity and the applied aerodynamic load, during the flapping stroke, it is determined whether the torque/power is positive or negative. If the aerodynamic load and wing velocity are in opposite directions (downstroke), then the aerodynamic load produces negative work into the system and extracts energy. This is the same as stating that the motor inputs positive work into the system and supplies energy. If the aerodynamic load and wing velocity are in the same direction (upstroke), then the aerodynamic load inputs positive work into the system and supplies energy. From the perspective of the motor, energy is absorbed from the aerodynamic load and negative work results.

The power balance is derived from Eg.(14), while keeping $\dot{\theta}$ intact and converting the linear velocity $\vec{V}_F$ to $f\dot{\phi}_{flap}$:

$$\tau_{m1}\dot{\theta} = F_{aero} f \dot{\phi}_{flap}. \tag{16}$$

The mechanical advantage (MA) is determined from the ratio of output load to input load of Eq.(16):

$$MA = \frac{M_{aero}}{\tau_{m1}} = \frac{\dot{\theta}}{\dot{\phi}_{flap}}, \tag{17}$$

where $\dot{\phi}_{flap}$ is the derivative of the flapping angle Eg.(6) with respect to θ. During the downstroke, the slider is driven upwards and the wing spar is driven downwards. The opposite scenario occurs during the upstroke, which demonstrates the flip in mechanical advantage throughout the cycle. The toggle positions at crank angle 90° and 270° exhibit zero torque. The peak torques occur at the locations of minimum mechanical advantage (0°, 180°, and 360°).

2. The Extension Spring Mechanism

The same process of virtual work, from the rigid body analysis is used to derive the equation of motor torque for the extension spring mechanism. Using this equation, the peak torque will be minimized through the use of numerical optimization. The design variables of the extension spring to be optimized are the attachment position of the spring along the wing spar r, the free length of the spring L_0, and the spring stiffness k.

Using the principle of virtual work, the following equation is obtained:

$$\delta W = \tau_{m2}\dot{\theta}\delta t + \vec{F}_{aero} \cdot \vec{V}_F \delta t + \vec{F}_{spring} \cdot \vec{V}_S \delta t = 0, \tag{18}$$

where the spring force is calculated as $\vec{F}_{spring} = -\vec{U}_{SD} k \Delta L$. And the linear velocity of position $\vec{P}_S$ is determined by taking the derivative of Eq.(8) with respect to θ.

The required motor torque for the extension mechanism is determined from Eq.(18) as

$$\tau_{m2}(\theta) = \frac{-\vec{F}_{aero} \cdot \vec{V}_F - \vec{F}_{spring} \cdot \vec{V}_S}{\dot{\theta}}, \quad \theta \in [0, 2\pi]. \tag{19}$$

3. The Compliant Joint Mechanism

As discussed previously, the compliant joint is analyzed using the pseudo-rigid-body model. In other words, the compliant joint is treated as a torsion spring between the two rigid linkages of the mechanism. The design parameters to be optimized are the initial torsion spring angle β_0 and the spring constant k. The virtual work equation for the torsion spring is

$$\delta W = \tau_{m3}\dot{\theta}\delta t + \vec{F}_{aero} \cdot \vec{V}_F \delta t + M_{spring}\dot{\beta}\delta t = 0, \tag{20}$$

where the moment of the torsion spring is defined as $M_{spring} = -k\Delta\beta$. And the angular velocity of β is the derivative of Eq.(10) with respect to θ.

From Eq.(20) the motor torque for the compliant joint mechanism is calculated as

$$\tau_{m3}(\theta) = \frac{-\vec{F}_{aero} \cdot \vec{V}_F - M_{spring}\dot{\beta}}{\dot{\theta}}, \quad \theta \in [0, 2\pi]. \tag{21}$$

B. Design Optimization of Compliant Mechanisms

The optimization was executed using an interior point algorithm in Wolfram Mathematica. Two functions were defined to calculate the motor torque at any point during the flap cycle for the extension spring mechanism and the compliant joint mechanism using Eqs. (19) and (21). The input arguments to these functions were the mechanism parameters such as link lengths and angles, the design parameters (spring stiffness, spring length and point of attachment of the spring) and the crank angle. The objective was to minimize the maximum torque to be produced by the motor during a single flap cycle as the crank angle varies between 0 and 2π.

A function $FindMinMax$ was defined in Mathematica using the built-in function $FindMinimum$ to perform the optimization. $FindMinimum$ works on an interior point algorithm. The setup of the optimization problem is discussed in detail in the following sections.

1. *The Extension Spring Mechanism*

Since the objective is to minimize the peak torque on the motor, the torque function from Eq.(19) is used in the objective function. The design variables are the attachment of point of the spring along the wing spar r and the free length of the spring L_0 and the spring constant k. The ranges for the design parameters were chosen after a preliminary inspection of the mechanism. L_0 and r were varied between $15mm$ and $24mm$ and k between $0N/mm$ and $0.9N/mm$.

Minimize

$$f_1(L_0, r, k) = \max_{\theta \in [0,2\pi]} |\tau_{m2}(L_0, r, k, \mathbf{y}, \theta)|$$

subject to

$$15 < L_0 < 24; \quad 15 < r < 24; \quad 0 < k < 0.9,$$

where $\mathbf{y}$ are other mechanism parameters shown in Fig. 1.

Optimization Results The optimized values were found to be $r = 24mm$, $k = 0.10334N/mm$, and $L_0 = 20.5535mm$. The peak torque of the optimized extension spring mechanism is $0.78425Nmm$, where as the peak torque of the rigid body mechanism is $7.3Nmm$. This is a 89.25% decrease in the required input torque from the motor.

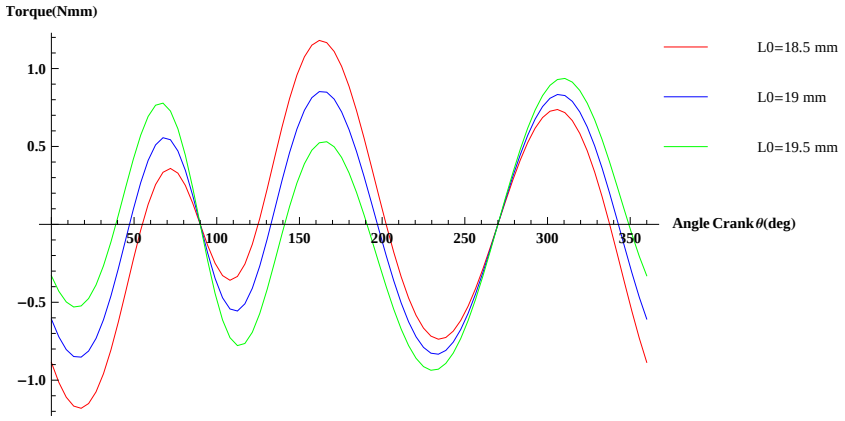

Figure 4. Minimized Peak Torque for Extension Spring Mechanism with Range of L_0

The details of how the spring free length affect the motor torque are shown in Figure 4. Here the torque is plotted for three different values $L_0 = 18.5mm$, $19mm$ and $19.5mm$. At the lower limit of the range ($L_0 = 18.5mm$), more spring force is generated due to the increase in pre-load. In the rigid body mechanism, the peak torque due to the aerodynamic load was at a crank angle of 0°, 180°, and 360°. The spring pre-load exceeds the magnitude of the aerodynamic load and results in these new peak torques. Most noticeably, there is positive work from the motor during the upstroke to manage the spring load. In the case of $L_0 = 19.5mm$, the extra free length of the spring results in less force being generated at the crank angles associated with peak torque. A spring free length of $L_0 = 19mm$ results in a peak torque at a crank angle of 162°. Here, the moment generated by the spring opposes the motor by dominating the aerodynamic load.

The final set of optimized parameters results in the torque plot captured in Figure 5. The peak torque resides at a crank angle of 162°, where the spring force acts against the motor thereby increasing the torque during the upstroke. In other words, the spring load dominates over the aerodynamic load, which causes a spike in motor torque. The spring was attached to the wing spar, such that the spring was at free length at the start of the downstroke, and fully stretch at the end of the upstroke. This allowed the extension spring to store the positive work of the aerodynamic load during the upstroke, instead of the motor absorbing it.

At the start of the downstroke, the extension spring releases the stored elastic energy to assist the motor, and reduce the peak torque.

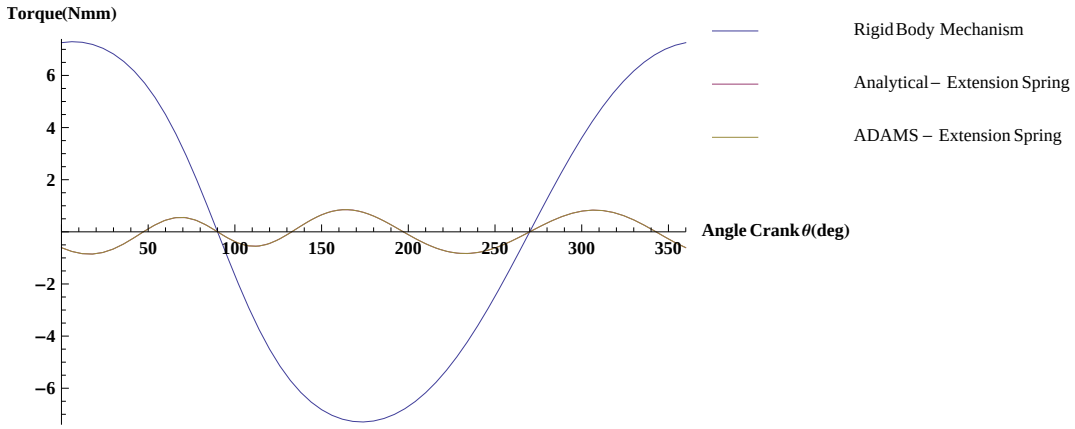

Figure 5. Minimized Peak Torque for Extension Spring Mechanism

2. The Compliant Joint Mechanism

The objective function of the optimization problem for the compliant joint mechanism uses the torque function from Eq.(21). Since the compliant joint acts like a torsion spring, the design parameters are the initial spring angle β_0 and the spring stiffness k.The range of β_0 is $-0.5rad$ to $0.4rad$. The negative angle allows for pre-load of the spring. The range of the spring constant k is $5Nmm/rad$ to $14Nmm/rad$.

Minimize

$$f_2(\beta_0, k) = \max_{\theta \in [0,2\pi]} |\tau_{m2}(\beta_0, k, \mathbf{y}, \theta)|$$

subject to

$$-0.5 < \beta_0 < 0.4; \quad 5 < k < 14$$

where $\mathbf{y}$ are other mechanism parameters shown in Fig. 1.

Optimization Results The minimized peak torque is $0.211Nmm$, and the optimized design parameters are $\beta_0 = -0.2784rad$ and $k = 7.0396Nmm/rad$, as seen in Fig. 6. This is a 97.1% decrease in torque from the rigid body mechanism, and a 73% reduction from the extension spring mechanism.

The change in torque for the range of β_0 is seen in Fig. 7. The lower limit ($\beta_0 = -0.35rad$), results in a spring pre-load which dominates, at the critical crank angles, over the aerodynamic load. The upper limit ($\beta_0 = -0.25rad$), also results in a pre-load, but is not large enough to completely oppose the aerodynamic load. At 306°, the peak torque results for $\beta_0 = -0.29rad$. This is due to a difference in convergence of the aerodynamic load and torsion spring load after the toggle position at 270°. After the compliant joint dominates the aerodynamic load near the critical angle of 180°, the aerodynamic load just passes the compliant load in magnitude after the toggle position.

IV. Discussion and Summary

The University of Maryland's Small Bird MAV transmission has been analyzed first as a rigid body mechanism, then after incorporating an extension spring mechanism, and finally using a compliant joint mechanism. The motor torque was derived in terms of the crank angle θ and the geometric linkage parameters. Holding the kinematics of the mechanism constant, the design parameters of the extension spring and

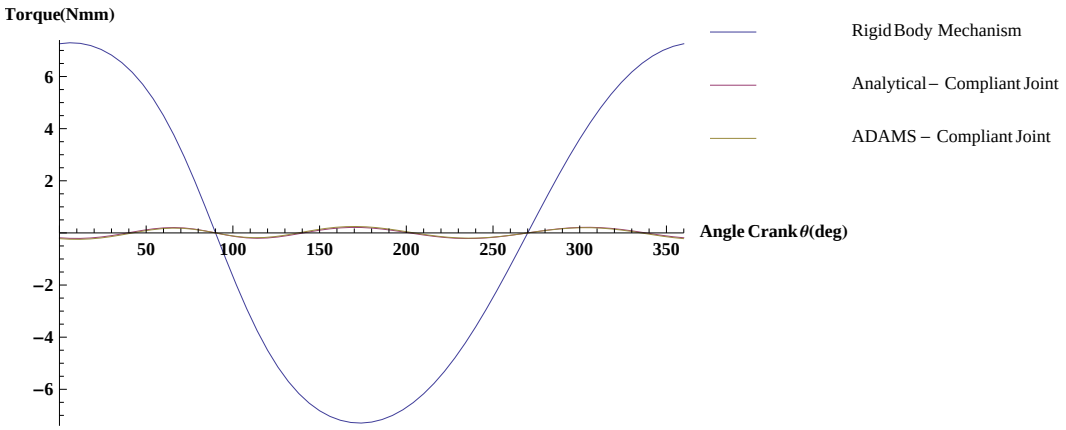

Figure 6. Minimized Peak Torque for Compliant Joint Mechanism

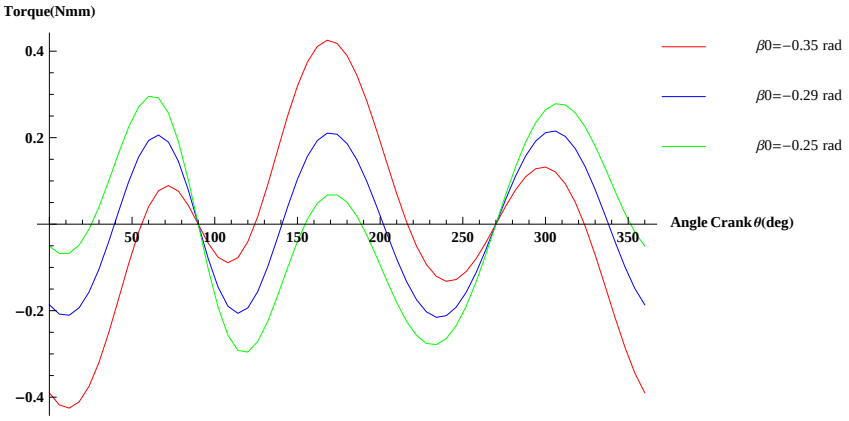

Figure 7. Minimized Peak Torque for Compliant Joint Mechanism with Range of β_0

compliant joint were optimized to minimize the maximum motor torque. The minimized motor torques are plotted in Fig. 8, and the dramatic improvement in power efficiency is easily recognizable.

The rigid body mechanism exhibited a peak torque of $7.3Nmm$ at a crank angle of 0°, 180°, and 360°. The optimization of the design parameters of the extension spring resulted in a peak torque of $0.7845Nmm$, which is a 89.25% reduction from the rigid body mechanism. The optimized design parameters of the extension spring are: $r = 24mm$, $L_0 = 20.5535mm$, and $k = 0.10334Nmm$. The spring was attached to the wing spar, such that the spring was at free length at the start of the downstroke, and fully stretch at the end of the upstroke. This allowed the extension spring to store the positive work of the aerodynamic load during the upstroke, instead of the motor absorbing it. At the start of the downstroke, the extension spring releases the stored elastic energy to assist the motor, and reduce the peak torque. The compliant joint mechanism operates on same principle of elastic energy storage during the upstroke, and energy release during the subsequent downstroke. However, the compliant joint mechanism achieved an even lower peak torque of $0.211Nmm$, which is a 97.1% decrease from the rigid body mechanism and a 73% decrease from the extension

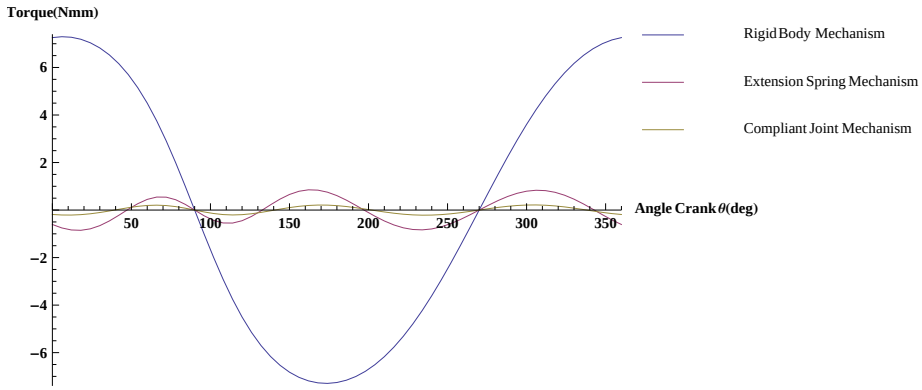

Figure 8. Motor Torque for Flapping Wing Mechanisms

spring mechanism. The optimized design parameters for the compliant joint are: $\beta_0 = -0.278404rad$ and $k = 7.0396Nmm/rad$.

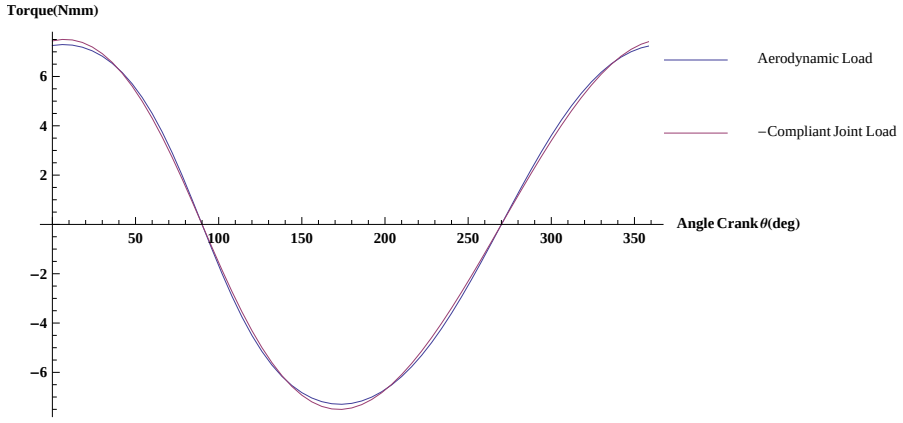

Figure 9. Aerodynamic Load vs. -Compliant Element Loads

The difference in these mechanisms is the manner in which the spring deforms and transfers its load to the wing spar. In Fig. 9, the moments due to the aerodynamic load and the negative of the moment due to the compliant elements are compared. The extension spring force is at a angle with the wing spar, and this angle changes throughout the flapping stroke. As this angle changes, the magnitude of the normal force to the wing spar also changes. The compliant joint relies purely on an angular deformation, which is directly related to the flapping angle. Since the compliant joint generates a moment about $\vec{P}_C$, and moves with $\vec{P}_C$, this design is more efficient.

The results of the use of compliant mechanisms to minimize the peak torque are in agreement with Tantanawat.[15] A four-bar linkage with and without an extension spring attached to the wing spar was analyzed with a similar constant upward and normal aerodynamic load. The extension spring resulted in a 84% reduction in peak input power for the motor.

Of course other solutions exist for minimizing the peak torque. An extension spring could be applied to the top of the slider, and thus eliminating the angle change deficiency present in the current design. Multiple

compliant joints could also be added to improve efficiency; however, the other revolute joints exhibit limited motion and therefore limited spring deformation. Short compliant segments are also possible, which are present in the original Small Bird MAV. Lastly, the geometric size of the linkages of the mechanism could also be optimized numerically; however, this was outside the scope of this study.

Limitations is this analysis include the simplified unidirectional aerodynamic load, ideal joints, massless links, and conservation of energy. A more accurate aerodynamic loading would provide insight into the mechanics required for actual flight. Out of plane loading and wing design are major factors to be considered when generating lift forces. In this analysis, it was assumed that the energy absorbed by the motor was fully recoverable. In actuality, this power would be dissipated by the motor and battery resistance.

V. Conclusions and Future Work

In this paper, we have demonstrated the use of elastic storage or compliant elements, in a flapping wing mechanism, as a way to minimize the peak motor torque. The University of Maryland's Small Bird MAV design has been selected as a test platform that is modified with an extension spring and a compliant joint. First, the mechanism is analyzed using rigid body mechanics, to determine the required motor torque in terms of the mechanism's geometric dimensions. Then the peak motor torque is minimized by optimizing the design parameters of the extension spring and compliant joint. This analysis will allow for direct comparison of a traditional rigid body mechanism, an extension spring mechanism, and a compliant joint mechanism. We conclude that the peak torque is reduced by 89.25% and 97.1% due to the use of extension and torsion springs. However this result is based on the assumption that the aerodynamic load on the wings is constant and energy can be fully absorbed and released by the motor. In the future, we will implement a higher fidelity aerodynamic force model and include other kinematic parameters of the linkages in the optimization process.

Acknowledgements

This work was sponsored by the Air Force Office of Scientific Research under contract AFOSR FA9550-12-1-0070. Opinions in this paper are those of the authors and do not necessarily reflect those of the sponsors.

References

[1]S. A. Ansari, R. bikowski, K. Knowles, Non-linear unsteady aerodynamic model for insect-like flapping wings in the hover. part 1: Methodology and analysis, Proceedings of the Institution of Mechanical Engineers, Part G: Journal of Aerospace Engineering 220 (2) (2006) 61–83.
URL http://pig.sagepub.com/content/220/2/61

[2]W. Bejgerowski, A. Ananthanarayanan, D. Mueller, S. K. Gupta, Integrated product and process design for a flapping wing drive mechanism, ASME Journal of Mechanical Design 131 (6) (2009) 061006–9.
URL http://link.aip.org/link/?JMD/131/061006/1

[3]W. Bejgerowski, J. W. Gerdes, S. K. Gupta, H. A. Bruck, S. Wilkerson, Design and fabrication of a multi-material compliant flapping wing drive mechanism for miniature air vehicles, ASME Conference Proceedings 2010 (44106) (2010) 69–80.
URL http://dx.doi.org/10.1115/DETC2010-28519

[4]L. L. Howell, Compliant Mechanisms, Wiley-Interscience, New York, NY, 2001.

[5]M. Keennon, K. Klingebiel, H. Won, A. Andriukov, Development of the nano hummingbird: A tailless flapping wing micro air vehicle, in: 50th AIAA Aerospace Sciences Meeting including the New Horizons Forum and Aerospace Exposition, Nashville, Tennessee, 2012.

[6]J. Khatait, S. Mukherjee, B. Seth, Compliant design for flapping mechanism: A minimum torque approach, Mechanism and Machine Theory 41 (1) (2006) 3–16.
URL http://www.sciencedirect.com/science/article/pii/S0094114X05001084

[7]A. Klaptocz, J.-D. Nicoud, D. Floreano, J.-C. Zufferey, M. Srinivasan, C. Ellington, Technology and fabrication of ultralight micro-aerial vehicles, in: Flying Insects and Robots, Springer Berlin Heidelberg, 2010, pp. 299–316.

[8]R. Madangopal, Z. A. Khan, S. K. Agrawal, Energetics-based design of small flapping-wing micro air vehicles, IEEE ASME Transactions On Mechatronics 11 (4) (2006) 433–438.

[9]J. M. McCarthy, Geometric Design of Linkages, Springer-Verlag, New York, NY, 2000.

[10]J. M. McMichael, M. S. Francis, Micro air vehicles - toward a new dimension in flight, DARPA document, available at http://www.fas.org/ irp/program/collect/docs/mav_auvsi.htm (1997).

[11]D. Mueller, J. Gerdes, D. Mueller, J. W. Gerdes, R. K. Gupta, Incorporation of passive wing folding in flapping wing miniature air vehicles, ASME Mechanism and Robotics Conference Proceedings (2009) 433–438.

[12]L. Petricca, P. Ohlckers, C. Grinde, Micro- and nano-air vehicles: State of the art, International Journal of Aerospace

Engineering 2011 (2011) 1–17.
URL http://www.hindawi.com/journals/ijae/2011/214549/

[13]M. Ryan, Design optimization and classi cation of compliant mechanisms for flapping wing micro air vehicles, Master's thesis, The Ohio State University (2012).

[14]M. Ryan, H.-J. Su, Classification of flapping wing mechanisms for micro air vehicles, in: Proceedings of ASME IDETC/CIE, 2012, chicago, IL, August 12-15.

[15]T. Tantanawat, S. Kota, Design of compliant mechanisms for minimizing input power in dynamic applications, ASME Journal of Mechanical Design 129 (10) (2007) 1064–1075.
URL http://dx.doi.org/10.1115/1.2756086